# A Central, Diamond-Staggered Dual Cell, Finite Volume Method for Ideal Magnetohydrodynamics

P. Arminjon[1] and R. Touma[2]

[1] Universit de Montral arminjon@crm.umontreal.ca
[2] Universit de Montral touma@dms.umontreal.ca

## 1 Introduction

The adaptation of shock capturing numerical methods to Magnetohydrodynamics (MHD) has been a very dynamic and continuous process since the early eighties; Since MHD plays an important role in astrophysical flows, which are highly compressible, it was soon observed that Godunov-type methods might be a useful approach to solve these problems. Among many important contributions let us mention Brio and Wu [3], Dai and Woodward [2].

In this paper we extend central Nessyahu-Tadmor-type one-dimensional [6] or multi-dimensional finite volume schemes to the resolution of some problems in ideal (inviscid and non-resistive) compressible Magnetohydrodynamics (MHD). In MHD, the interaction between magnetic and fluid dynamic phenomena is described by a set of eight equations [1]: one mass conservation law, three momentum conservation laws, one energy conservation law and Faraday's (three-dimensional) law for the magnetic field $\mathbf{B}$.

$$\frac{\partial}{\partial t}\begin{bmatrix}\rho\\ \rho\mathbf{u}\\ \rho e\\ \mathbf{B}\end{bmatrix} + \nabla\cdot\begin{bmatrix}\rho\mathbf{u}\\ \rho\mathbf{u}\mathbf{u} + I(p+\frac{\mathbf{B}\cdot\mathbf{B}}{2\mu_o}) - \frac{\mathbf{B}\mathbf{B}}{\mu_o}\\ (\rho e + p + \frac{\mathbf{B}\cdot\mathbf{B}}{2\mu_o})\mathbf{u} - \frac{1}{\mu_o}(\mathbf{u}\cdot\mathbf{B})\mathbf{B}\\ \mathbf{u}\mathbf{B} - \mathbf{B}\mathbf{u}\end{bmatrix} = 0 \tag{1}$$

where $\rho, \mathbf{u}, p, \mathbf{B}$ and $e$ are the mass density, velocity field vector, thermal pressure, magnetic field vector and the specific total energy. $\mu_o$ is the permeability of the vacuum and $I$ is the $(3\times 3)$ identity matrix. This system of equations is completed by the equation of state $p = (\gamma-1)\rho\epsilon$, where $\gamma$ is the ratio of specific heats and $\epsilon$ denotes the specific internal energy.

## 2 Two-Dimensional Cartesian Diamond-Staggered Scheme

We consider the two-dimensional hyperbolic system of conservation laws:

$$\overrightarrow{U}_t + \nabla\cdot\overrightarrow{F}(\overrightarrow{U}) \equiv \overrightarrow{U}_t + \overrightarrow{f}_x + \overrightarrow{g}_y = 0 \tag{2}$$

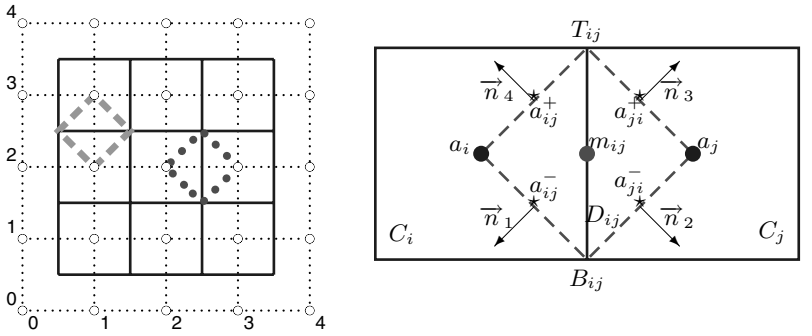


**Fig. 1.** (Left) Square cell centers denoted by 'o', dual oblique cells in red (dotted) and green (dashed); (Right) Original cells $C_i, C_j$ and the dual cell $D_{ij}$; case when $a_i a_j$ is parallel to the $x$-axis

with the initial condition $\overrightarrow{U}(x, y, 0) = \overrightarrow{U_o}(x, y)$. We consider for our computational domain a uniform rectangular grid with $M^2$ square cells. Starting from the original Cartesian grid with cells $C_i$ at time $t^n$, we alternate to the diamond dual cell $D_{ij}$ at time $t^{n+1}$, and return back to the original cell $C_i$ of the original structured grid as shown in Fig.1. Let $\Delta x = \Delta y = h = x_{i+1/2} - x_{i-1/2}$ denote the mesh size, $(x_i, y_j) = (ih, jh), 0 \leq i, j \leq M$, denote the nodes of the first grid. We consider a numbering of the nodes "$a_i$", $1 \leq i \leq (M+1)(M+1)$; for any arbitrary node $a_i$ we consider the corresponding finite volume cell $C_i$ for the first grid to be the square centered at $a_i$ with sides parallel to the axes as in Fig.1. The diamond dual cells $D_{ij}$ are shown in Fig.1. There are 2 cases depending on whether the axis joining the two nodes of the original grid used to define the diamond cell is parallel to the $x-$axis (the "i-j" or the "$x$-direction" case) or to the $y-$axis (the "i-k" or the "$y-$direction" case). In Fig.1 the dual cell (in the $x - direction$) is the quadrilateral $a_i T_{ij} a_j B_{ij}$. Nodes of the staggered grid are the centroids of the diamond cells. Let $\overrightarrow{U}_i^n \cong \overrightarrow{U}(a_i, t^n)$ and $\overrightarrow{U}_{ij}^{n+1} \cong \overrightarrow{U}(m_{ij}, t^{n+1})$ denote respectively the average values in the first and second grid at time $t^n$ and $t^{n+1}$. Performing the first time step gives $\overrightarrow{U}_{ij}^{n+1}$ (n even), while the cell values $\{\overrightarrow{U}_i^{n+2}\}$ are obtained at the end of the second time step.

As can be seen in Fig.1, the first time step should be performed by successively scanning in the $x$ and $y$ directions, in order to cover the whole computational domain. We consider here two adjacent nodes $a_i$ and $a_j$, where $a_i a_j$ is parallel to the $x-$axis, and $D_{ij}$ denotes the corresponding dual cell. Integrating (2) on $D_{ij} \times [t^n, t^{n+1}]$:

$$\int_{t^n}^{t^{n+1}} \iint_{D_{ij}} \overrightarrow{U}_t dA dt = -\int_{t^n}^{t^{n+1}} \iint_{D_{ij}} \nabla \cdot \overrightarrow{F} dA dt \tag{3}$$

and applying Green's theorem gives,

$$\iint_{D_{ij}} \overrightarrow{U}(x,y,t^{n+1})dA = \iint_{D_{ij}} \overrightarrow{U}(x,y,t^{n})dA - \int_{t^n}^{t^{n+1}} \oint_{\partial D_{ij}} (\overrightarrow{f}\, n_x + \overrightarrow{g}\, n_y) d\sigma dt \quad (4)$$

where $\overrightarrow{n} = (n_x, n_y)$ is the unit outward normal vector to the boundary of the diamond cell $\partial D_{ij}$. The left-hand side of (4) defines the value $A(D_{ij})\overrightarrow{U}_{ij}^{n+1}$.

The first integral in the RHS of (4) is approximated to second order by

$$\iint_{D_{ij}} \overrightarrow{U}(x,y,t^{n})dA \cong \overrightarrow{U}(x_i + \frac{\Delta x}{3}, y_i, t^n)A(D_{ij} \cap C_i) + \overrightarrow{U}(x_j - \frac{\Delta x}{3}, y_j, t^n)A(D_{ij} \cap C_j) \quad (5)$$

Applying van Leer's piecewise linear interpolants will guarantee second-order accuracy and preserve the monotonicity. Using (5) then leads to

$$\begin{aligned}\iint_{D_{ij}} \overrightarrow{U}(x,y,t^{n})dA &\cong \overrightarrow{U}_i^n A(D_{ij} \cap C_i) + \overrightarrow{U}_j^n A(D_{ij} \cap C_j) \\ &+ \frac{1}{3}\overrightarrow{U}_{i,x}^{lim} A(D_{ij} \cap C_i) - \frac{1}{3}\overrightarrow{U}_{j,x}^{lim} A(D_{ij} \cap C_j) \\ &= \frac{h^2}{4}\big(\overrightarrow{U}_i^n + \overrightarrow{U}_j^n + \frac{1}{3}\overrightarrow{U}_{i,x}^{lim} - \frac{1}{3}\overrightarrow{U}_{j,x}^{lim}\big) \quad (6)\end{aligned}$$

where $\nabla\overrightarrow{U}^{lim} = (\overrightarrow{U}_x^{lim}/\Delta x, \overrightarrow{U}_y^{lim}/\Delta y)$ is a limited numerical gradient. Using (6) and applying the midpoint rule to the flux-integral in (4) both in time and space finally leads to:

$$\begin{aligned}\overrightarrow{U}_{D_{ij}}^{n+1} = \frac{1}{2}(\overrightarrow{U}_i^n + \overrightarrow{U}_j^n) + \frac{1}{6}(\overrightarrow{U}_{i,x}^{lim} - \overrightarrow{U}_{j,x}^{lim}) - \frac{\Delta t}{h}\big[\big(-\overrightarrow{f}_{a_{ij}^-}^{n+1/2} - \overrightarrow{g}_{a_{ij}^-}^{n+1/2}\big) \\ + \big(\overrightarrow{f}_{a_{ji}^-}^{n+1/2} - \overrightarrow{g}_{a_{ji}^-}^{n+1/2}\big) + \big(\overrightarrow{f}_{a_{ji}^+}^{n+1/2} + \overrightarrow{g}_{a_{ji}^+}^{n+1/2}\big) + \big(-\overrightarrow{f}_{a_{ij}^+}^{n+1/2} + \overrightarrow{g}_{a_{ij}^+}^{n+1/2}\big)\big]\end{aligned}$$

where $(\overrightarrow{f}_{a_{ij}^{\pm}}^{n+1/2})$ are values predicted at time $t^{n+1/2}$, using (2) and an explicit Euler time discretization. For a description of the second time step, see [7].

## 3 The divB=0 Constraint and Numerical Experiments.

It is shown in electromagnetic theory that the magnetic field vector $\mathbf{B}$ must be solenoidal, and thus satisfy Maxwell's equation $\nabla \cdot \mathbf{B} = 0$. If the initial magnetic field satisfies the corresponding divergence-free constraint $(\nabla \cdot \mathbf{B}|_{t=0} = 0)$, Faraday's law ensures that it remains divergence-free for all subsequent time. On the other hand, due to the accumulation of errors, the

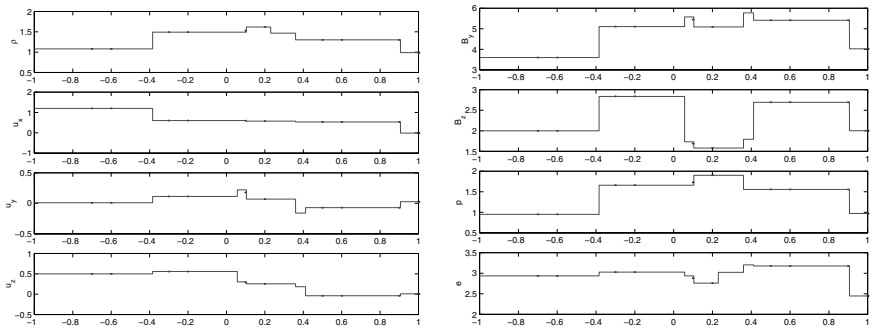

**Fig. 2.** One-dimensional MHD shock tube problem, MC-($\theta = 2$) limiter

numerical solution will tend to lose track of this constraint, leading to a non-solenoidal magnetic field, which in turn can lead to serious losses in accuracy, non-physical waves, and to the production of negative pressure and density in the ideal MHD case. Inspired from [4], we have constructed a method to enforce the $\nabla \cdot \mathbf{B} = 0$ constraint in the case of staggered Central Schemes, which we call the CTCS method ("Constrained Transport for Central Schemes"). See [7] for details. The CTCS applies indifferently to central schemes with Cartesian grids, 2 and 3-D diamond dual cells and Unstructured triangular or tetrahedric grids.

We first solved the 1-D MHD shock tube problem. We use the interval [-1,1] of the $x-$axis, let $\gamma = 5/3, B_x = 2$ and consider the initial data for the Riemann problem at $x = 0$, $U_r = [0.989112, -0.013123, 0.026933, 0.010037, 4.024421, 2.002600, 0.971588]$ and $U_l = [1.08, 1.2, 0.01, 0.5, 3.6, 2.0, 0.95]$ with $U = [\rho, u_x, u_y, u_z, B_y, B_z, p]$. Numerical results are compared with the exact solution of this problem presented in [3].This first test case features seven discontinuities. We have considered a grid with 1000 meshpoints. The solution is computed at time $t = 0.25$ along with a CFL condition of 0.485. Fig.2 shows a very good agreement between the numerical and exact solutions. We then solved a 2D-adaptation of the one-dimensional MHD shock tube problem, involving a compound wave, which consists of a shock and, directly attached, a rarefaction wave. The computational domain is the rectangle $-1 \leq x \leq 1, 0 \leq y \leq 1$. The initial conditions feature a shock along the axis $x = 0$ with the following data: $U_l = [1, 0, 0, 0, \sqrt{4\pi}, 0, 1]$, $Ur = [0.125, 0, 0, 0, -\sqrt{4\pi}, 0, 0.1]$, and $B_x = 0.75\sqrt{4\pi}$. The solution is computed at time $t = 0.25$ with a CFL condition of 0.485. The computations were performed with an MC-$\theta$ ($\theta = 1.5$) limiter. Fig.3 shows a good agreement of the numerical solution (400 data points dotted in blue) with the solution of the corresponding one-dimensional problem obtained from a Riemann solver (10000 data points, solid red line). For our second 2D problem, we consider a Riemann problem where the four initial states $(\rho, p, u_x, u_y)$ are

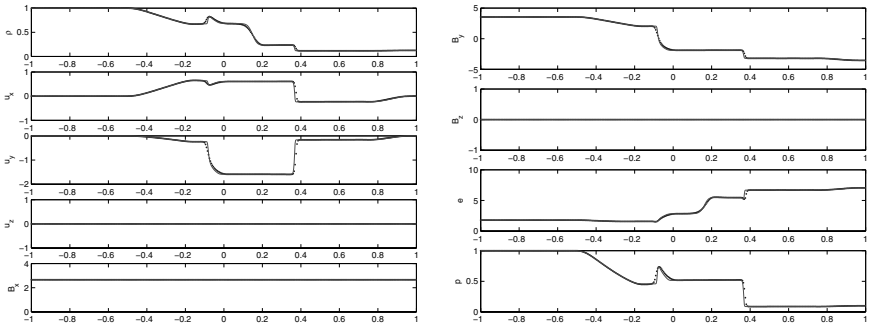

**Fig. 3.** Two-dimensional MHD shock tube problem, MC-($\theta = 1.5$) limiter

$(1, 1, 0.75, 0.5)$ for $x > 0$ and $y > 0$, (2,1,0.75,0.5) for $x < 0$ and $y > 0$, (1,1,-0.75,0.5) for $x < 0$ and $y < 0$ and (3,1,-0.75,-0.5) for $x > 0$ and $y < 0$. We consider a uniform initial magnetic field $\mathbf{B} = (2, 0, 1)$. The solution is computed at time $t = 0.6175$ on a 300×300 grid. Fig.4 shows the contour lines for mass density and energy, respectively. Here again our numerical results are similar to those presented in [2]. For our final 2D test, we consider the Orszag-Tang MHD vortex problem. The initial conditions for our example are: $\rho(x, y) = \rho_0, p(x, y) = p_0\mathbf{u}(x, y) = -\sin(2\pi y)\mathbf{i} + \sin(\mathbf{2}\pi\mathbf{x})\mathbf{j}, \mathbf{B}(\mathbf{x}, \mathbf{y}) = -\sin(\mathbf{2}\pi\mathbf{y})\mathbf{i} + \sin(\mathbf{4}\pi\mathbf{x})\mathbf{j}$ with $\rho_0 = 25/(36\pi)$ and $p_0 = 5/(12\pi)$. $\mathbf{i}$ and $\mathbf{j}$ are unit vectors in the $x-$ and $y-$ directions. Fig.5 shows the mass density contours at time $t = 0.5$ (left) and $t = 2$ (right).

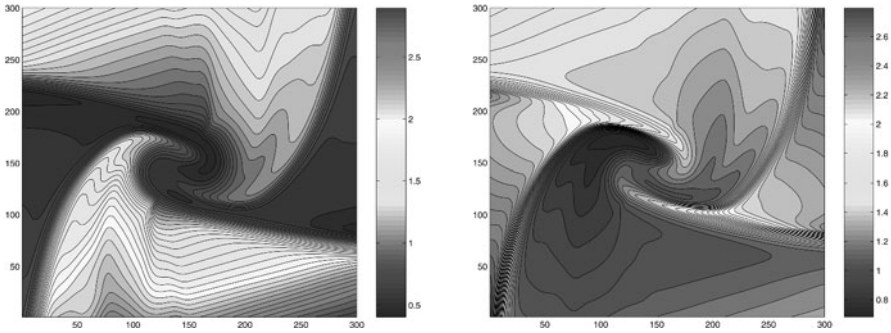

**Fig. 4.** Two-dimensional MHD Riemann problem

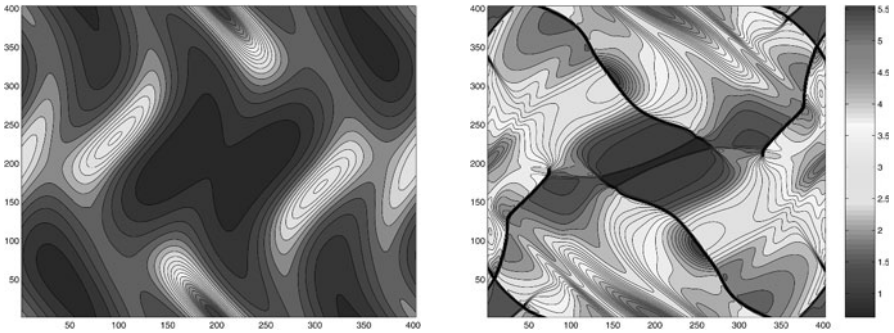


**Fig. 5.** Two-dimensional Orszag-Tang MHD turbulence problem, MC-($\theta = 1.5$) limiter

## 4 Conclusion

In this paper, we have extended our Nessyahu-Tadmor-type central finite volume methods to one and two-dimensional MHD problems, using Cartesian cells for the original grid, and our previously introduced diamond cells for the dual grid. The resolution of the Riemann problems at the cell interfaces is by-passed by central schemes, leading to computing time reductions. Our results show the high potential of the method which was robust enough to allow us to avoid, in a first attempt, the use of a strategy to maintain the div·$\mathbf{B}$=0 constraint. For more elaborate numerical tests, we found it necessary to construct a method to satisfy this constraint, suitably designed to be applied in the context of our staggered central schemes. Using this method the constraint was satisfied to 10e-14 accuracy and we obtain results (Fig.5) identical with those appearing in the literature. For a description of our method to satisfy the div·$\mathbf{B}$=0 constraint and more numerical tests see [7].

## References

1. L. D. Landau, E. Lifshitz: *Electrodynamics of Continuous Media*, (Pergamon, New York, 1960)
2. W. Dai and P.R. Woodward: J. Comp. Phys. **142**, 331 (1998)
3. M. Brio, C.C. Wu: J. Comp. Phys. **75**, 400 (1988)
4. C. R. Evans and J. F. Hawley: Appl. Phys. Astrophys. J. **332**, 659 (1988)
5. G. Tóth: J. Comp. Phys. **161**, 605 (2000)
6. H. Nessyahu, E. Tadmor: J. Comp. Phys. 2 **87**, 408 (1990)
7. P. Arminjon and R. Touma: preprint submitted to App. Num. Math. (2004)
8. P. Arminjon and R. Touma: Central Finite Volume Methods for one and two-dimensional ideal magnetohydrodynamics. In: *12th Annual Conference of the CFD Society of Canada*, ed by S. Chen, S. Mcllwain, 585 (2004)